Available online at www.sciencedirect.com
SCIENCE DIRECT®
Mathematics and Computers in Simulation 66 (2004) 297–314
MATHEMATICS AND COMPUTERS IN SIMULATION
www.elsevier.com/locate/matcom

Multifrequency inverse obstacle scattering: the point source method and generalized filtered backprojection

D. Russell Luke*,[1]

Department of Mathematics, Simon Fraser University, Burnaby, BC, Canada V5A 1S6

This work is dedicated to Rainer Kress in honor of his 60th birthday, with deep gratitude for his support and encouragement

Available online 25 March 2004

Abstract

We outline two methods for obstacle reconstruction from multifrequency far-field scattering data, the first built upon the point source method proposed by Potthast for solving inverse scattering problems with single frequency data in the resonance region, and the second based on filtered backprojection techniques using the physical optics approximation for high frequency scattering. Our implementation using the point source method can be viewed as a generalized filtered backprojection algorithm, the key to which is the construction of the filter used in the backprojection operator. Numerical examples illustrate that the critical factor for reconstructions in multifrequency settings is the frequency dependence of the filter.

Keywords: Inverse problems; Scattering theory; Image processing

1. Introduction

In recent years, many innovative algorithms have appeared for inverse scattering applications in the resonance region. Of particular interest here are algorithms that share the feature of splitting the original ill-posed non-linear inverse problem into an ill-posed linear inverse problem, and a well-posed non-linear problem. These algorithms were designed primarily with single, low-frequency applications in mind. Good examples can be found in the pioneering work of Colton and Monk [6,7], Kirsch and Kress [10], Colton and Kirsch [4], and Potthast [18]. In the present work, we study one of the above methods in the context of a classical high-frequency technique that employs the physical optics approximation. In this short space, it is impossible to do justice to all of the above techniques, so we limit our scope to the point source method proposed by Potthast [18]. The multifrequency aspect of our investigation is

* Tel.: +1-604-224-3569; fax: +1-604-291-4947.
E-mail address: rluke@cecm.sfu.ca (D.R. Luke).
[1] This work was written while the author was at the University of Göttingen, and was supported in part by a Post-Doctoral Fellowship from the Pacific Institute for the Mathematical Sciences.

0378-4754/$30.00 © 2004 IMACS. Published by Elsevier B.V. All rights reserved.
doi:10.1016/j.matcom.2004.02.009

not specific to the point source method, however, it serves to underscore the power of this essentially non-linear technique in comparison with much simpler and coarse filtered backprojection based on the physical optics approximation.

We begin with a brief orientation to forward scattering. Inverse scattering, including the point source method and physical optics approximations, is treated in Section 3. Our discussion of the point source method focuses mainly on the approximation of the scattered field. For more detail on the theory and implementation, interested readers are referred to [19,20]. Numerical results are presented in Section 4.

2. Forward scattering

This discussion is limited to scattering of small-amplitude, monochromatic, time-harmonic waves from an impenetrable, sound-soft obstacle embedded in an isotropic homogeneous medium. The obstacle is identified by its support $\Omega \subset \mathbb{R}^m$, $m = 2$ or 3. Throughout this work, unless otherwise stated, Ω is assumed to be a bounded domain with connected C^2 (twice continuously differentiable) boundary $\partial\Omega$ and the unit outward normal ν. The governing equation for this setting is the Helmholtz equation:

$$(\Delta + \kappa^2)v(x) = 0, \quad x \in \bar{\Omega}^c \subset \mathbb{R}^m, \tag{1}$$

where Δ denotes the Laplacian, $\kappa \geq 0$ is the *frequency* or *wavenumber* and $\bar{\Omega}^c := \mathbb{R}^m \backslash \bar{\Omega}$. Our analysis is built upon the principle of superposition of single, fixed frequencies. To limit notational clutter, we therefore omit any explicit dependency on the wavenumber κ and simply denote solutions to Eq. (1) as complex-valued scalar mappings $v : \bar{\Omega}^c \to \mathbb{C}$. If there is any chance for confusion, we denote the wave v at x parameterized by the wavenumber κ as $v(x, k)$ and consider this a mapping on the product space $v : \bar{\Omega}^c \times \mathbb{R}_+ \to \mathbb{C}$. The surface of the obstacle is assumed to be perfectly absorbing or sound-soft. This is modeled with Dirichlet boundary conditions: $v = f$ on $\partial\Omega$ where, f is continuous on $\partial\Omega$.

Consider an *incident* field $v^i : \mathbb{R}^m \to \mathbb{C}$ that, for fixed κ, is an *entire solution* to the Helmholtz equation on $\mathbb{R}^m$, that is v^i satisfies Eq. (1) on $\mathbb{R}^m$. The *scattering problem* is to find the *total field* $v : \Omega^c \to \mathbb{C}$ that satisfies Eq. (1) on $\bar{\Omega}^c$ and $v = v^i + v^s$ with $f = 0$ for the boundary condition, and where $v^s : \Omega^c \to \mathbb{C}$ is the *scattered field* satisfying Eq. (1) on $\bar{\Omega}^c$ and the *Sommerfeld radiation condition*:

$$r^{(m-1)/2}\left(\frac{\partial}{\partial r} - \mathrm{i}\kappa\right)v^s(x) \to 0, \quad r = |x| \to \infty, \tag{2}$$

uniformly in all directions. The scattering problem has a unique solution [5]. At large distances from the obstacle Ω, the scattered field v^s is characterized by the *far-field pattern* $v^\infty : \mathbb{S} \to \mathbb{C}$ on the set of directions $\mathbb{S} := \{x \in \mathbb{R}^m || x| = 1\}$. We denote the direction of a vector $x \in \mathbb{R}^m$ by $\hat{x} := x/|x|$.

For fixed $\kappa > 0$ let $v^s \in C^2(\bar{\Omega}^c) \cap C(\Omega^c)$ satisfy Eqs. (1) and (2) with Dirichlet boundary conditions. Denote the free-space fundamental solution to Eq. (1) by $\Phi : \mathbb{R}^m \times \mathbb{R}^m \to \mathbb{C}$ (see Eqs. (2.1) and (3.60) in [5]). Then v^s satisfies Green's formula (Eq. (2.5) in [5]), also known as the Integral Theorem of Kirchhoff and Helmholtz, for $x \in \bar{\Omega}^c$ and $\kappa > 0$ Let v be the corresponding solution to the scattering problem for a sound-soft scatterer (i.e. $v = 0$ on $\partial\Omega$) with entire incident wave v^i. Then $v(x) = v^i(x) + v^s(x)$, $x \in \bar{\Omega}^c$, $\kappa > 0$, and Green's formula applied to v^s, together with the application of Green's Theorem applied to v^i and Φ, yield the following formalization of Huygens' principle (Theorem 3.12 in [5]):

$$v^s(x) = -\int_{\partial\Omega} \frac{\partial v(z)}{\partial \nu(z)} \Phi(x, z)\, \mathrm{d}s(z), \quad x \in \bar{\Omega}^c. \tag{3}$$

The corresponding far-field pattern is given by:

$$v^\infty(\hat{x}) = -\beta \int_{\partial\Omega} \frac{\partial v(z)}{\partial \nu(z)} \mathrm{e}^{-\mathrm{i}\kappa \hat{x}\cdot z}\, \mathrm{d}s(z), \quad \hat{x} \in \mathbb{S}, \tag{4}$$

where β is given by (Eqs. (2.13) and (3.64) in [5]):

$$\beta = \frac{\mathrm{e}^{-\mathrm{i}(\pi/4)}}{\sqrt{8\pi\kappa}} \quad \text{for} \quad m = 2 \quad \text{and} \quad \beta = \frac{1}{4\pi} \quad \text{for} \quad m = 3. \tag{5}$$

Note that in two dimensions, β is a function of κ, unlike the three-dimensional setting. The *far-field mapping* $T_{\Omega_\alpha} : v^{\mathrm{s}}|\Omega_\alpha \to v^\infty$ maps the scattered field v^{s} restricted to any compact subset $\Omega_\alpha \subset \bar{\Omega}^{\mathrm{c}}$ containing open subsets to the far-field v^∞. This is a continuous mapping. We reserve special notation for incident *plane waves* denoted by:

$$u^{\mathrm{i}}(x, \hat{\eta}) := \mathrm{e}^{\mathrm{i}\kappa x\cdot\hat{\eta}}, \quad x \in \mathbb{R}^m, \quad \hat{\eta} \in \mathbb{S}. \tag{6}$$

Here, $\hat{\eta} \in \mathbb{S}$, indicates the *direction of incidence*.

3. Inverse scattering

Let $\Gamma \subset \mathbb{S}$ denote an open set of directions on $\mathbb{S}$. Here, Γ models the aperture on which our sensors lie. In our numerical experiments, this is a symmetric interval of the unit sphere centered with respect to the direction of the incident field. The far-field u^∞ due to an incident plane wave with direction $\hat{\eta} \in \mathbb{S}$ is measured at points $\hat{y} \in \Gamma$. Define the operator $\tilde{H}_\kappa : L^2(-\Gamma) \to L^\infty(\mathbb{R}^m)$ by:

$$(\tilde{H}_\kappa g)(x) := \int_\Gamma \mathrm{e}^{\mathrm{i}\kappa x(-\hat{y})} g(-\hat{y})\, \mathrm{d}s(\hat{y}), \quad x \in \mathbb{R}^m, \quad g \in L^2(-\Gamma). \tag{7}$$

It is shown in Lemma 2.1 in [15] that the operator $\tilde{H}_\kappa$ is injective with dense range for almost every κ. The corresponding family of functions parameterized by κ and mapping $\mathbb{R}^m$ to $\mathbb{C}$, $\tilde{h}_g := (\tilde{H}_\kappa g)(\cdot)$, consists of entire solutions to the Helmholtz equation. Note that the function g is only defined on $-\Gamma$ where $-\Gamma$ is the mirror image of the interval Γ on the unit sphere: $\hat{y} \in \Gamma \Leftrightarrow -\hat{y} \in -\Gamma$. When the aperture is the entire sphere, $\Gamma = \mathbb{S}$, then we denote the corresponding function, also known as the Herglotz wave function ([5], p. 55), by h_g. In contrast to the density g for limited apertures, the far-field due to scattering from an incident plane wave u^∞ is defined on Γ with any incident wave direction $\hat{\eta}$. The region $-\Gamma$ defines a *virtual* aperture corresponding to the physical aperture Γ on which the sensors lie. Looking ahead to filtered backprojection, the virtual aperture in the case of scattering is analogous to the actual measurement array in X-ray transmission tomography. For example, in classical parallel scanning X-ray tomography, a source with direction $-\hat{\eta}$ emitted from the point $\hat{\eta} \in \Gamma$ has a corresponding receiver located at the point $-\hat{\eta} \in -\Gamma$.

3.1. The point source method

The next theorem establishes the central principle behind the point source method. Here, the duality of incident point sources and incident plane waves is used to construct a backprojection operator mapping the far-field due to an incident plane wave to the corresponding scattered field at an arbitrary point z in the

near field. In fact, we construct a *family* of backprojection operators with kernel $g(\cdot, z, \kappa)$ parameterized by the location $z \in \mathbb{R}^m$ and wavenumber $\kappa \in \mathbb{R}_+$ of the field to be reconstructed. To make clear the source of the dependence on z and κ we write the family of backprojection operators as mappings on the product space $\mathcal{A}_g : L^2(\Gamma \times \mathbb{R}_+) \to L^2(\mathbb{R}^m \times \mathbb{R}_+)$:

$$(\mathcal{A}_g \psi)(z, \kappa) := \int_\Gamma \psi(\hat{y}, \kappa) \frac{g(-\hat{y}, z, \kappa)}{\beta(\kappa)} \, \mathrm{d}s(\hat{y}), \quad \psi \in L^2(\Gamma \times \mathbb{R}_+), \tag{8}$$

for $\beta(\kappa)$ given by Eq. (5). The construction of such a backprojection operator relies on the approximation of the fundamental solution Φ at frequency κ due to a point source at the point z by the function:

$$\tilde{h}_g(x, z, \kappa) := (\tilde{H}_\kappa g(-\hat{y}, z, \kappa))(x) = \int_\Gamma \mathrm{e}^{\mathrm{i}\kappa x(-\hat{y})} g(-\hat{y}, z, \kappa) \, \mathrm{d}s(\hat{y}), \tag{9}$$

for $x \in \mathbb{R}^m$, $g(\cdot, z, \kappa) \in L^2(-\Gamma)$. Surely we cannot hope to approximate Φ *everywhere*, but it can be shown that if we choose the density g such that $\tilde{h}_g$ approximates Φ on the C^2 boundary of a bounded, connected domain Ω_a satisfying $\bar{\Omega} \subset \Omega_a$, then $\mathcal{A}_g$ with kernel g operating on $u^\infty(\hat{y}, \hat{\eta})$ will approximate the scattered field $u^\mathrm{s}(z, \hat{\eta})$. Theorem 1 is a restatement of Theorem 2.1 in [15], which includes the limited aperture setting; the original idea in the full aperture setting is due to Potthast and can be found in [18,20]. As usual, the explicit dependence of the operators and functions on κ is dropped for notational ease since κ is fixed.

Theorem 1 (Backprojection). *Let $\Omega_a \subset \mathbb{R}^m$ be a bounded domain (the domain of approximation) with connected C^2 boundary such that $\bar{\Omega} \subset \Omega_a$. For the fixed wavenumber $\kappa > 0$, assume that κ^2 is not a Dirichlet eigenvalue of the negative Laplacian on the interior of Ω_a. Denote the fundamental solution to Eq. (1) with singularity at $z \in \mathbb{R}^m \backslash \bar{\Omega}_a$ by $\Phi(\cdot, z)$, and let the function $\tilde{h}_g(\cdot, z) : \mathbb{R}^m \to \mathbb{C}$ be defined by Eq. (9). Given any $\delta > 0$, there exists an $\epsilon > 0$ such that, for all $g(\cdot, z) \in L^2(-\Gamma)$ satisfying:*

$$||\Phi(\cdot, z) - \tilde{h}_g(\cdot, z)||_{C(\partial\Omega_a)} < \varepsilon, \tag{10}$$

we have

$$|u^\mathrm{s}(z, \hat{\eta}) - (\mathcal{A}_g u^\infty)(z, \hat{\eta})| < \delta, \tag{11}$$

where u^s and u^∞ are the scattered field and far-field pattern due to an incident plane wave with direction $\hat{\eta} \in \mathbb{S}$ and $\mathcal{A}_g$ is defined by Eq. (8).

Proof of Theorem 1. By the injectivity and denseness of the range of the operator $\tilde{H}_\kappa$ on $\partial\Omega_a$ (Lemma 2.1 in [15]), there exists a function $\tilde{h}_g$ satisfying Eq. (10). Let $v : \mathbb{R}^m \to \mathbb{C}$ be a solution to the scattering problem on Ω with incident field $v^i = \tilde{h}_g(\cdot, z)$. Then both v^i and Φ solve Eq. (1) on the interior of Ω_a. By the continuity of Φ and v^i on $\bar{\Omega}_a$, given any δ', there is an ϵ such that Eq. (10) implies:

$$||\Phi(\cdot, z) - v^\mathrm{i}||_{C(\bar{\Omega}_a)} < \delta', \quad \text{and hence} \quad ||\Phi(\cdot, z) - \tilde{h}_g(\cdot, z)||_{C(\partial\Omega)} < \delta'. \tag{12}$$

On $\partial\Omega$, $v^\mathrm{s} = -\tilde{h}_g$ and $w^\mathrm{s}(\cdot, z) = -\Phi(\cdot, z)$ where w^s is the scattered field due to an incident point source. Thus, since the far-field mapping, $\mathcal{T}_{\partial\Omega}$, from v^s to v^∞ is a continuous mapping, there exists a δ' such that, given any δ, $||w^\mathrm{s}(\cdot, z) - v^\mathrm{s}||_{C(\partial\Omega)} < \delta'$ implies:

$$|w^\infty(-\hat{\eta}, z) - v^\infty(-\hat{\eta}, z)| < \delta, \quad \forall -\hat{\eta} \in \mathbb{S}. \tag{13}$$

By Lemma 3.16 in [5]:

$$v^{\infty}(-\hat{\eta}, z) = \int_{\Lambda} u^{\infty}(-\hat{\eta}, -\hat{y})\, g(-\hat{y}, z)\, \mathrm{d}s(\hat{y}), \tag{14}$$

where u^{∞} is the far-field pattern due to scattering of an incident plane wave. Now, w^{∞} is related to u^{s} via the *mixed reciprocity relation* [11]:

$$w^{\infty}(-\hat{\eta}, z) = \beta u^{\mathrm{s}}(z, \hat{\eta}), \quad \hat{\eta} \in \mathbb{S}, \quad z \in \mathbb{R}^m \backslash \bar{\Omega}_a. \tag{15}$$

This, together with the standard reciprocity relation $u^{\infty}(\hat{y}, \hat{\eta}) = u^{\infty}(-\hat{\eta}, -\hat{y})$ (see Theorem 3.13 in [5]), yields the result:

$$\left| u^{\mathrm{s}}(z, \hat{\eta}) - \int_{\Gamma} u^{\infty}(\hat{y}, \hat{\eta}) \frac{g(-\hat{y}, z)}{\beta}\, \mathrm{d}s(\hat{y}) \right| < \delta.$$

□

For an incident plane wave of fixed direction $\hat{\eta}$, the point source method involves approximating the scattered field u^{s} *at every point* z in the computational domain using the backprojection operator $\mathcal{A}_g$ with density $g(\cdot, z)$. By Theorem 1, the approximation Eq. (11) depends on the construction of $g(\cdot, z)$ at every z to satisfy Eq. (10). There are many possibilities for calculating g depending on the size of the parameter ϵ and the choice of the domain of approximation Ω_a. The approximating domain need not—indeed *will not*—be the same for every point z. Neither will the condition $\Omega \subset \Omega_a$ be satisfied for every domain of approximation since the precise location and size of the object Ω is not known. In Section 3.2, we derive rough estimates for g based on high-frequency physical optics approximations that do not rely on an approximating domain Ω_a. Before discussing this technique, we review an optimization approach for calculating g originally proposed by Potthast [18,20] for the case of full aperture scattering.

The density we select, denoted $g_*(\cdot, z, \kappa)$ or simply $g_*(\cdot, z)$, is the one that, for a fixed frequency κ and fixed point z, solves a regularized least squares minimization problem. Recall that when $\Gamma = \mathbb{S}$ we write $h_g = \tilde{h}_g$ for $\tilde{h}_g$ defined by Eq. (9). The restriction to a limited aperture $\Gamma \subset \mathbb{S}$ is treated as a penalty in the objective of the following optimization problem:

$$\text{minimize } ||\Phi(\cdot, z) - h_g(\cdot, z)||^2_{L^2(\partial\Omega_a)} + \alpha ||g(\cdot, z)||^2_{L^2(\mathbb{S})} + \tilde{\alpha} ||(1 - \mathcal{X}_{-\Gamma}) g(\cdot, z)||^2_{L^2(\mathbb{S})}, \tag{16}$$

over $g(\cdot, z) \in L^2(\mathbb{S})$ where $\mathcal{X}_{-\Gamma}$ is the indicator function for the reflected aperture $-\Gamma$, that is $\mathcal{X}_{-\Gamma}(\hat{y}) = 1$ for $\hat{y} \in -\Gamma$ and $\mathcal{X}_{-\Gamma}(\hat{y}) = 0$ otherwise.

The first challenge is to choose the appropriate domain of approximation Ω_a and regularization parameters α and $\tilde{\alpha}$ without knowing exactly where or how large the obstacle is. To do this, we create a generating domain Ω_0 for a point source located at $z = 0$, and then calculate the corresponding density $g_*(\cdot, 0)$ satisfying Eq. (16). The spatial invariance of the fundamental solution allows one to *scan* the computational domain by translations of Ω_0. The density $g_*(\cdot, z)$ corresponding to the translated generating domain can be written explicitly in terms of $g_*(\cdot, 0)$ as Proposition 1 shows.

Proposition 1. *Let Ω_0 be any bounded test domain in $\mathbb{R}^m \backslash \{0\}$ with connected C^2 boundary and for which κ is not an eigenvalue for the interior Dirichlet problem. Consider the problem*:

$$\text{minimize } ||\Phi(\cdot, 0) - h_g(\cdot, 0)||^2_{L^2(\partial\Omega_0)} + \alpha_0 ||g(\cdot, 0)||^2_{L^2(\mathbb{S})} + \tilde{\alpha}_0 ||(1 - \mathcal{X}_{-\Gamma}) g(\cdot, 0)||^2_{L^2(\mathbb{S})}, \tag{17}$$

over $g(\cdot,0) \in L^2(\mathbb{S})$ *where the function* h_g *is the extension to* $\mathbb{S}$ *of* $\tilde{h}_g$ *defined by* Eq. (9). *This problem has a unique solution* $g_*(\cdot,0)$. *Moreover, the optimal solution to the problem*:

$$\text{minimize } ||\Phi(\cdot,z) - h_g(\cdot,z)||^2_{L^2(\partial(\Omega_0+z))} + \alpha_0||g(\cdot,z)||^2_{L^2(\mathbb{S})} + \tilde{\alpha}_0||(1-\mathcal{X}_{-\Gamma})g(\cdot,z)||^2_{L^2(\mathbb{S})}, \tag{18}$$

over $g(\cdot,z) \in L^2(\mathbb{S})$ *is given by*:

$$g_*(\hat{y},z) = \mathrm{e}^{-\mathrm{i}\kappa z\cdot\hat{y}} g_*(\hat{y},0), \quad \hat{y} \in \mathbb{S}. \tag{19}$$

Proof of Proposition 1. The objective function in Eq. (17) is a uniformly convex functional, and $L^2(\mathbb{S})$ is complete, hence existence and uniqueness of solutions follows from standard results in optimization theory.

To prove the second statement, note that the norms on the space $L^2(\mathbb{S})$ are invariant under multiplication by the complex factor $\mathrm{e}^{\mathrm{i}\kappa z\cdot\hat{y}}$; so one need only show that:

$$||\Phi(\cdot,0) - h_*(\cdot,0)||^2_{L^2(\partial\Omega_0)} = ||\Phi(\cdot,z) - h_*(\cdot,z)||^2_{L^2(\partial(\Omega_0+z))},$$

where $h_*(\cdot,0)$ denotes the Herglotz wave function with kernel $g_*(\cdot,0)$, a solution to Eq. (17), and with $g_*(\cdot,z)$ given by Eq. (19). To see this, define $h'_*(x,z)$ by:

$$h'_*(x,z) := \int_{\mathbb{S}} \mathrm{e}^{\mathrm{i}\kappa x(-\hat{y})} g'_*(-\hat{y},z)\,\mathrm{d}s(\hat{y}),$$

for $g'_*(-\hat{y},z) = \mathrm{e}^{\mathrm{i}\kappa z(-\hat{y})} g_*(-\hat{y},z)$. Note that $h_*(x,z) = h'_*(x-z,z)$. By the spatial invariance of the fundamental solution, $\Phi(x,z) = \Phi(x-z,0)$, which yields:

$$\begin{aligned} ||\Phi(\cdot,z) - h_*(\cdot,z)||^2_{L^2(\partial(\Omega_0+z))} &= ||\Phi(\cdot,-z,0) - h'_*(\cdot,-z,z)||^2_{L^2(\partial(\Omega_0+z))} \\ &= ||\Omega(\cdot,0) - h'_*(\cdot,z)||^2_{L^2(\partial(\Omega_0))} \geq ||\Phi(\cdot,0) - h_*(\cdot,0)||^2_{L^2(\partial(\Omega_0))}. \end{aligned} \tag{20}$$

Now, since $g_*(\hat{y},0)$ is the optimal solution to Eq. (17), equality holds in Eq. (20) if $h'_*(x,z) = h_*(x,0)$, that is, if:

$$g'_*(\hat{y},z) = \mathrm{e}^{\mathrm{i}\kappa z\cdot\hat{y}} g_*(\hat{y},z) = g_*(\hat{y},0),$$

which is what we set out to prove. □

As a consequence of Theorem 1, one need solve the optimization problem (Eq. (16)) once for the generating domain of approximation Ω_0. The solution to Eq. (17) can be written explicitly as the solution to the normal equations. For details see [15,18,20]. The backprojection operator given by Eq. (8) corresponding to these translated domains can be written in terms of the generating density $g_*(\cdot,0)$ as:

$$(\tilde{\mathcal{A}}_{g_*}u^\infty)(z,\hat{\eta}) := \int_\Gamma u^\infty(\hat{x},\hat{\eta}) \frac{g_*(-\hat{x},0)}{\beta} \mathrm{e}^{-\mathrm{i}\kappa z(-\hat{x})}\,\mathrm{d}s(\hat{x}), \quad z \in \mathbb{R}^m. \tag{21}$$

The points z satisfying the hypotheses of Theorem 1 depend on the geometry of this generating domain and that of the scatterer Ω. Where the hypotheses are not satisfied, the behavior of the function represented in Eq. (21) is in general unpredictable, though it is often observed that the pointwise values are large [15,16,18,20]. The domain of approximation that we use is shown in Fig. 1(a). This domain is chosen in particular to allow us to exploit the radial symmetry of point sources.

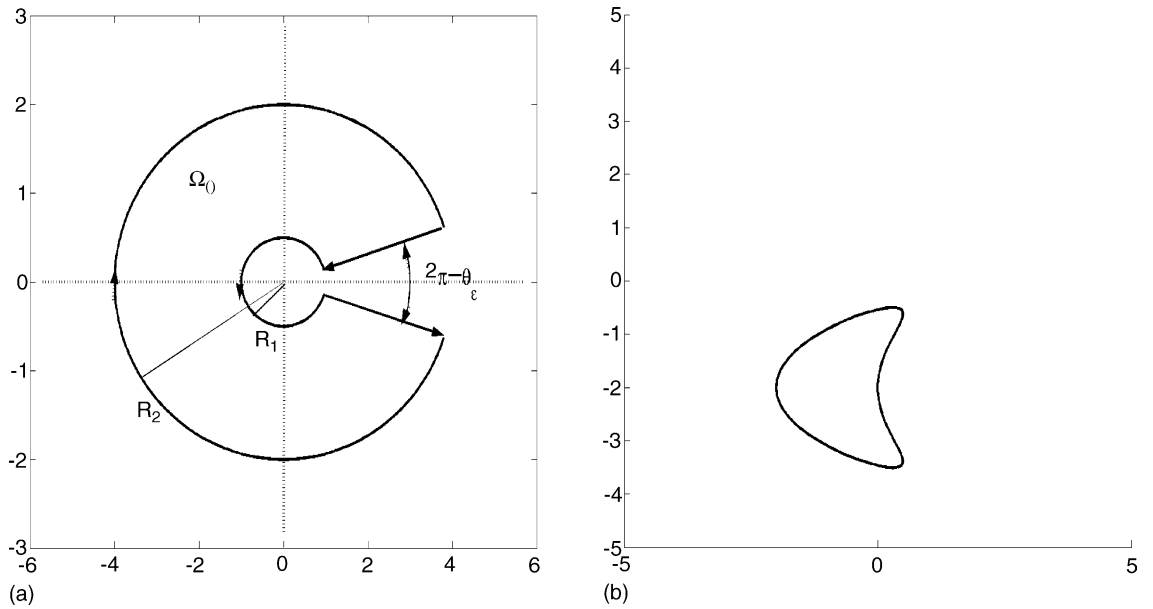

Fig. 1. (a) Domain of approximation Ω_a. (b) Scattering obstacle.

3.2. Physical optics and filtered backprojection

The high frequency asymptotics of the far-field pattern yield a variety of shape reconstruction techniques. In this section, we briefly review the well-known Fourier inversion method for reconstructing sound-soft scatterers based on the classical *physical optics* or *Kirchhoff* approximation. Our description is terse. The usual justification for Fourier inversion is limited to *convex* obstacles [3], however, with some further assumptions on the regularity of Ω, this can be extended to weakly non-convex obstacles [2,12].

To begin, let $u^{\mathrm{i}}(\cdot, \hat{\eta})$ be an incident plane wave with direction $\hat{\eta}$. Define $\partial\Omega_+$ to be the illuminated side of the scattering domain $\partial\Omega_+ := \{x \in \partial\Omega | \nu(x) \cdot \hat{\eta} < 0\}$. The shadow of the scattering domain, $\partial\Omega_-$, is defined as $\partial\Omega_- := \partial\Omega \backslash \overline{\partial\Omega}_+$. The physical optics or Kirchhoff approximation is written:

$$\frac{\partial u^{\mathrm{s}}(x,\hat{\eta})}{\partial \nu(x)} \approx \begin{cases} \dfrac{\partial u^{\mathrm{i}}(x,\hat{\eta})}{\partial \nu(x)}, & x \in \partial\Omega_+ \\ -\dfrac{\partial u^{\mathrm{i}}(x,\hat{\eta})}{\partial \nu(x)}, & x \in \partial\Omega_- \end{cases}, \quad \kappa \gg 0. \tag{22}$$

In words, for large κ (that is, small wavelengths), the obstacle can be locally approximated by a plane, and the scattered field behaves accordingly. The physical optics approximation is to obstacle scattering what the Fresnel approximation is to diffraction (see Section 3.1.1 in [14]). Explicit upper bounds on the error are beyond the scope of this work. Suffice it to say that the accuracy of the approximation depends essentially on a small angle argument. For more detailed asymptotics, interested readers are referred to

Lies (Section 8 in [12]) and references therein. Substituting Eq. (22) into Eq. (3) yields the identity:

$$u^{\mathrm{s}}(x,\hat{\eta}) \approx -2\int_{\partial\Omega_+} \frac{\partial u^{\mathrm{i}}(z,\hat{\eta})}{\partial \nu(z)} \Phi(x,z)\,\mathrm{d}s(z), \quad \kappa \gg 0. \tag{23}$$

The corresponding far-field pattern thus has the following asymptotic behavior with respect to the wavenumber:

$$u^{\infty}(\hat{x},\hat{\eta}) \approx -2\beta(\kappa)\int_{\partial\Omega_+} \frac{\partial u^{\mathrm{i}}(z,\hat{\eta})}{\partial \nu(z)} \mathrm{e}^{-\mathrm{i}\kappa\hat{x}\cdot z}\,\mathrm{d}s(z), \tag{24}$$

for $\hat{x},\hat{\eta} \in \mathbb{S}$ and $\kappa(\hat{x}-\hat{\eta}) \gg 0$. Note that, in this case, the approximation is asymptotically valid for $\kappa(\hat{x}-\hat{\eta}) \gg 0$, not just when $\kappa \gg 0$. In particular, if $\hat{x} \approx \hat{\eta}$, that is at points in the far-field in or near the shadow of the obstacle, the non-linear effects of scattering are strong and hence the physical optics approximation is only valid at very large wavenumbers. Likewise, on the shadow of Ω we have:

$$u^{\infty}(\hat{x},-\hat{\eta}) \approx 2\beta(\kappa)\int_{\partial\Omega_-} \frac{\partial u^{\mathrm{i}}(z,-\hat{\eta})}{\partial \nu(z)}\, \mathrm{e}^{-\mathrm{i}\kappa\hat{x}\cdot z}\,\mathrm{d}s(z). \tag{25}$$

Let $\hat{\mathcal{X}}_\Omega$ denote the Fourier transform of the indicator function of the obstacle Ω:

$$\hat{\mathcal{X}}_\Omega(\xi) := \frac{1}{(2\pi)^{m/2}}\int_{\mathbb{R}^m} \mathcal{X}(z)\,\mathrm{e}^{-\mathrm{i}\xi\cdot z}\,\mathrm{d}z,$$

with $\mathcal{X}_\Omega(z)$ the indicator function of the scatterer Ω. Then, Green's *first* theorem (Eq. (2.2) in [5]), together with Eqs. (24) and (25) for $\kappa(\hat{x}-\hat{\eta}) \gg 0$, yield:

$$u^{\infty}(\hat{x},\hat{\eta}) + \overline{u^{\infty}(-\hat{x},-\hat{\eta})} \approx -2\beta(\kappa)\int_{\partial\Omega} \frac{\partial u^{\mathrm{i}}(z,\hat{\eta})}{\partial \nu(z)}\, \mathrm{e}^{-\mathrm{i}\kappa\hat{x}\cdot z}\,\mathrm{d}s(z) + R(\hat{x},\hat{\eta}), \tag{26}$$

$$= 2(2\pi)^{m/2}\beta(\kappa)\,\kappa^2(1-\hat{\eta}\cdot\hat{x})\,\hat{\mathcal{X}}_\Omega(\kappa(\hat{x}-\hat{\eta})) + R(\hat{x},\hat{\eta}), \tag{27}$$

where

$$R(\hat{x},\hat{\eta}) = 4\mathrm{i}\,\mathrm{Im}(\beta(\kappa))\int_{\partial\Omega_-} \frac{\partial u^{\mathrm{i}}(z,\hat{\eta})}{\partial \nu(z)}\, \mathrm{e}^{-\mathrm{i}\kappa\hat{x}\cdot z}\,\mathrm{d}s(z). \tag{28}$$

Rearranging terms in Eq. (27) yields:

$$\left(u^{\infty}(\hat{x},\hat{\eta}) + \overline{u^{\infty}(-\hat{x},-\hat{\eta})}\right)\frac{\tilde{g}(\kappa)}{\beta(\kappa)} \approx (1-\hat{\eta}\cdot\hat{x})\,\hat{\mathcal{X}}_\Omega(\kappa(\hat{x}-\hat{\eta})) + \frac{\tilde{g}(\kappa)}{\beta(\kappa)}R(\hat{x},\hat{\eta}), \tag{29}$$

with

$$\tilde{g}(\kappa) := \frac{1}{2(2\pi)^{m/2}\kappa^2}, \quad m = 2,3. \tag{30}$$

The dependence of the approximations on $\hat{x}$ and $\hat{\eta}$ as well as κ is clear with the term $(1-\hat{\eta}\cdot\hat{x})$ in Eqs. (27) and (29). Indeed, at $\hat{x} = \hat{\eta}$ the approximation predicts that the far-field is zero. Also note that in $\mathbb{R}^3$ the factor $\beta(\kappa)$ is real (see Eq. (5)), so the term involving the integral R vanishes. In this case, it is apparent

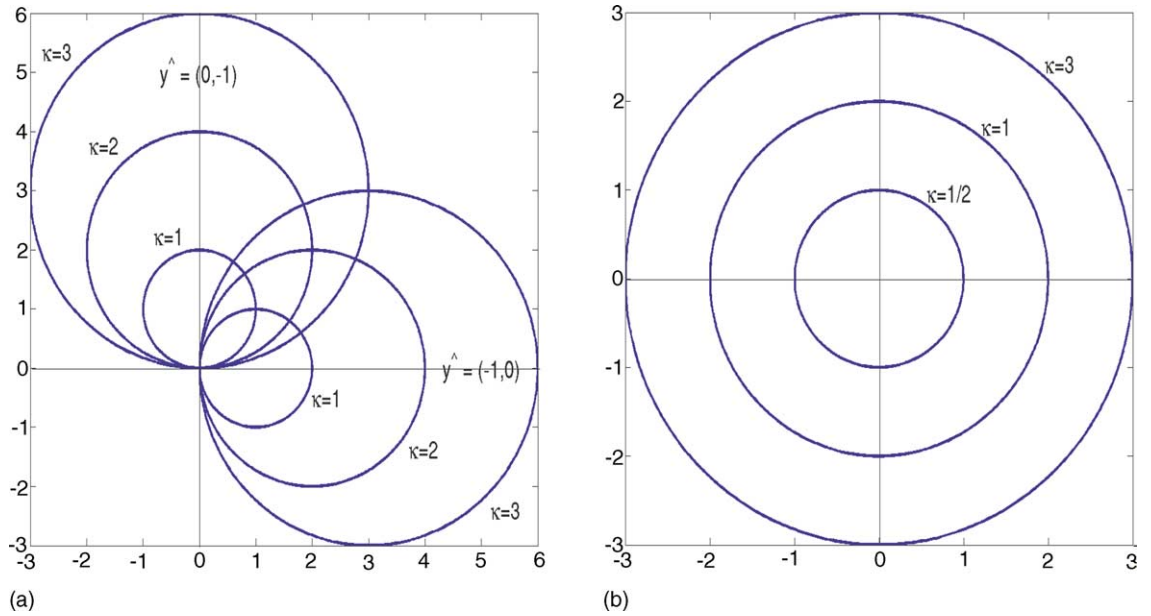

Fig. 2. Scattering data geometry for $\mathbb{R}^2$. (a) Full scattering data for two incident directions. (b) Backscatter only for all incident directions.

from Eq. (29) that for a fixed incident direction $\hat{\eta}$, the far-field data at wavenumber κ, $u^\infty(\hat{x}, \hat{\eta})$, lies in the spatial frequency domain along a sphere of radius κ with center $-\kappa\hat{\eta}/2$. This is illustrated in Fig. 2(a) for three wavenumbers and two incident field directions. It is clear from Fig. 2(a) that one requires a sufficient number of incident fields and/or wavelengths to adequately "cover" the spatial frequency domain in order to recover $\mathcal{X}_\Omega$ by Fourier inversion. There is some redundancy, however, in the data in the case where data from all wavenumbers and all incident directions is collected. This redundancy has been noted in the case of scattering from inhomogeneous media in [21]. Fig. 2(a) serves as a graphical heuristic for a uniqueness theorem proven by Colton and Sleeman [8] which states that the scattering problem with Dirichlet boundary data is unique, given a finite number of incident fields depending on the wavenumber κ and the size of the scatterer.

We rewrite Eq. (29) in terms of the backprojection operator $\tilde{\mathcal{A}}_{\tilde{g}}$ (see Eq. (21)) with kernel $\tilde{g}$ (see Eq. (30)) by multiplying both sides of Eq. (29) by $\mathrm{e}^{\mathrm{i}\kappa\hat{x}\cdot z}$ and integrating with respect to $\hat{x}$ over the aperture Γ:

$$(\tilde{\mathcal{A}}_{\tilde{g}}u^\infty)(z,\hat{\eta}) + (\tilde{\mathcal{A}}_{\tilde{g}}\tilde{u})(z,\hat{\eta}) \approx \int_\Gamma (1-\hat{\eta}\cdot\hat{x})\,\hat{\mathcal{X}}_\Omega(\kappa(\hat{x}-\hat{\eta}))\,\mathrm{e}^{\mathrm{i}\kappa\hat{x}\cdot z}\,\mathrm{d}s(\hat{x}) + (\tilde{\mathcal{A}}_{\tilde{g}}R)(z,\hat{\eta}), \tag{31}$$

with $\tilde{u}(\hat{x},\hat{\eta}) := \overline{u^\infty(-\hat{x},-\hat{\eta})}$. Unlike the density g_* satisfying Eq. (17), the density $\tilde{g}$ does not depend on a domain of approximation Ω_0 or the point of approximation z. For points $z \in \Omega^{\mathrm{c}}$ satisfying $\Omega \subset \Omega_0 + z$ for any Ω_0, wherever $\tilde{g}$ satisfies Eq. (10) for $\epsilon > 0$ large enough, the backprojection operator $\tilde{\mathcal{A}}_{\tilde{g}}$ applied to the far-field data $u^\infty(\hat{x},\hat{\eta})$ approximates the scattered field $u^{\mathrm{s}}(z,\hat{\eta})$ with upper bounds on the pointwise error given by Eq. (11). Thus, the physical optics approximation yields an easily calculated density whose dependence on the wavenumber κ is *explicit*. This is discussed next.

3.3. Special case: backscattering

We finish this discussion of inverse scattering techniques by examining the special case of reconstructions by a single far-field data measurement $u^\infty(\hat{y}, \hat{\eta}, \kappa)$ for each incident field with direction $\hat{\eta}$ and wavenumber κ, $u^{\mathrm{i}}(x, \hat{\eta}, \kappa)$. We do not omit the dependence on κ here since this emphasizes the critical difference between the filter suggested by the physical optics approximation and that calculated by the point source method. The limited aperture is a single point $\Gamma = \{\hat{y}\}$. For an incident field with direction $\hat{\eta}$, the aperture $\{\hat{y}\} = \{-\hat{\eta}\}$ corresponds to *backscattered* data. This case illustrates the key differences between the density g calculated as the solution to Eq. (17), or some related optimization problem, and the density $\tilde{g}$ predicted by the physical optics approximation (Eq. (30)). We begin with the physical optics approximation.

For simplicity, we consider only scattering in $\mathbb{R}^3$. Here, Eq. (27) simplifies to:

$$\left(u^\infty(-\hat{\eta}, \hat{\eta}, \kappa) + \overline{u^\infty(\hat{\eta}, -\hat{\eta}, \kappa)}\right) \frac{\tilde{g}(\kappa)}{\beta(\kappa)} \approx 2\hat{\mathcal{X}}_\Omega(-2\kappa\hat{\eta}). \tag{32}$$

Note that, for fixed wavelength κ, the data u^∞ is collected along a sphere in the spatial frequency domain with radius 2κ (see Fig. 2(b)). This is reminiscent of the radon transform, where the Fourier Slice Theorem (Theorem 2.1.1 in [17]) relates the Fourier transform in polar coordinates to the Radon transform. Indeed, by this interpretation, the factor $\tilde{g}$ is a *filter* in the standard filtered backprojection algorithm for inverting the Radon transform. This connection between scattering and generalized Radon transformation is well known. Interested readers are referred to [13] for details.

For the integrals over the aperture $\Gamma = \{-\hat{\eta}\}$ in Eq. (31) to be meaningful in the case of backscattering (in particular, Eq. (9) and all related integral operators) we interpret the density g as a *distribution*. Here, we include the dependence on κ, $g(\hat{y}, z, \kappa) = \delta(\hat{y} - \hat{\eta})\, c(z, \kappa)$, where $c : \mathbb{R}^m \times \mathbb{R}_+ \to \mathbb{C}$ and δ is the Dirac delta function. According to this interpretation, the density calculated by the physical optics approximation is given by:

$$\tilde{g}(\hat{y}, \kappa) = \frac{\delta(\hat{y} - \hat{\eta})}{2(2\pi)^{m/2}\kappa^2}, \quad m = 2, 3, \tag{33}$$

independent of the point $z \in \mathbb{R}^m$ or the approximation domain Ω_a. By Theorem 1, however, in order to achieve the best approximation (in the L^2 sense) to the scattered field u^{s} at the point z for a given generating approximation domain Ω_0 we seek an optimal choice for the constant c that yields the best approximation to the point source Φ on $\Omega_0 + z$ by the *backscattering* Herglotz wave operator $\tilde{H}$ given by Eq. (7) acting on the distribution g, that is, $(\tilde{H}g(\hat{y}, z, \kappa))(x) = \mathrm{e}^{\mathrm{i}\kappa x\cdot\hat{\eta}} c(z, \kappa)$. A similar argument to the Proof of Proposition 1 shows that the solution to the finite-dimensional optimization problem

$$\text{minimize } ||\Phi(\cdot, z, \kappa) - \mathrm{e}^{\mathrm{i}\kappa(\cdot)\hat{\eta}} c(z, \kappa)||^2_{L^2(\partial\Omega_0 + z)}, \tag{34}$$

over $c(z, \kappa) \in \mathbb{C}$, is given by $c_*(z, \kappa) = \mathrm{e}^{-\mathrm{i}\kappa z\cdot\hat{\eta}} c_*(0, \kappa)$ where $c_*(0, \kappa)$ is the optimal solution to:

$$\text{minimize } ||\Phi(\cdot, 0, \kappa) - \mathrm{e}^{\mathrm{i}\kappa(\cdot)\hat{\eta}} c(0, \kappa)||^2_{L^2(\partial\Omega_0)}, \tag{35}$$

over $c(0, \kappa) \in \mathbb{C}$.

A straight-forward calculation shows that the unique optimal solution to this problem is:

$$c_*(0, \kappa) = \frac{1}{\int_{\partial\Omega_0} \mathrm{d}s(x)} \left\langle \Phi(x, 0, \kappa), \mathrm{e}^{\mathrm{i}\kappa x\cdot\hat{\eta}} \right\rangle_{L^2(\partial\Omega_0)}, \tag{36}$$

with the corresponding optimal distribution given by:

$$g_*(\hat{y}, z, \kappa) = \delta(\hat{y} - \hat{\eta})\, \mathrm{e}^{-\mathrm{i}\kappa z\cdot\hat{\eta}} c_*(0, \kappa). \tag{37}$$

Note that $\tilde{g}$ behaves as κ^{-2} while the behavior of g_* is on the order of $\kappa^{1-m/2}$.

This is a critical difference for multifrequency data. In the next section we compare the results of reconstructions using both densities $\tilde{g}$ and g_*.

4. Results

4.1. Series representations

The optimization approach of Eq. (17) provides a means for explicitly constructing the density $g_*(\cdot, 0)$. We gain some insight into the behavior of $g_*(\cdot, 0)$ through elementary series expansions. For simplicity the discussion is limited to $\mathbb{R}^2$.

For a fixed point x and fixed wavenumber κ, write the function h_g defined by Eq. (9) in polar coordinates:

$$h_g(x, z) = \int_{\mathbb{S}} \mathrm{e}^{\mathrm{i}\kappa x(-\hat{y})} g(-\hat{y}, z)\, \mathrm{d}s(\hat{y}) = \int_0^{2\pi} \mathrm{e}^{-\mathrm{i}kr\cos(\theta-\phi)} g(-\phi, z)\, \mathrm{d}\phi, \tag{38}$$

for $x = r(\cos\theta, \sin\theta)$, and $\hat{y} = (\cos\phi, \sin\phi)$. Note that, as in Eq. (16), the restriction to a limited aperture $\Gamma \subset \mathbb{S}$ has been dropped in the formulation of the function h_g since this is treated as a penalty in the optimization problem associated with the construction of g. Since g is defined on the torus, it has a Fourier series expansion:

$$g(\phi, z) = \sum_{n=0}^{\infty} \hat{g}_n(z, \kappa)\, \mathrm{e}^{\mathrm{i}n\phi}, \quad \text{with} \quad \hat{g}_n(z, \kappa) = \int_0^{2\pi} g(\phi, z)\, \mathrm{e}^{\mathrm{i}n\phi}\, \mathrm{d}\phi.$$

Interchanging the sum and the integral yields:

$$h_g(x, z) = \sum_{n=0}^{\infty} \hat{g}_n(z, \kappa)\, W_n(\kappa r, \theta), \tag{39}$$

where

$$W_n(\kappa r, \theta) := \int_0^{2\pi} \mathrm{e}^{\mathrm{i}(n\phi + \kappa r\cos(\theta-\phi)}\, \mathrm{d}\phi. \tag{40}$$

The substitution $\omega = \theta - \phi + \pi/2$ [9, Eq. (8.411.1)] yields:

$$W_n(\kappa r, \theta) = 2\pi \mathrm{e}^{\mathrm{i}n(\theta+(\pi/2))} J_n(\kappa r), \tag{41}$$

where J_n is the Bessel function of order $n \in \mathbb{N}$.

As described in Proposition 1, the generating domain Ω_0 is constructed relative to a fundamental solution centered at the origin, $z = 0$. It is not important at this point what the domain of approximation Ω_0 is, as long as it does not contain the origin, and the wavenumber κ is not a Dirichlet eigenvalue on

the interior of Ω_0. In polar coordinates the centered fundamental solution on $\mathbb{R}^2$ is a scaled, zero-order Hankel function of the first kind:

$$\Phi(r) = \tfrac{1}{4}\mathrm{i}(J_0(\kappa r) + \mathrm{i}Y_0(\kappa r)), \tag{42}$$

where Y_0 is the Neumann function of order zero (Eq. (3.60) in [5]). The Fourier coefficients of the truncated series representation for $g_*(\cdot, 0)$ are calculated as the solution to the following finite-dimensional least squares optimization problem with respect to the vector of coefficients:

$$\text{minimize } ||\Phi(r) - \mathcal{W}_N(\kappa r, \theta) \cdot \hat{g}(0, \kappa)||^2_{L^2(\partial\Omega_0)} + \alpha_0||\hat{g}(0, \kappa)||^2_{\mathbb{R}^N} + \tilde{\alpha}_0||\mathcal{T}_N(\phi) \cdot \hat{g}(0, \kappa)||^2_{L^2(\mathbb{S})}, \tag{43}$$

over $\hat{g}(0, \kappa) = (\hat{g}_0(0), \hat{g}_1(0), \ldots, \hat{g}_N(0)) \in \mathbb{C}^{N+1}$. Here, $\mathcal{W}_N$ is the vector of functions, $\mathcal{W}_N(\kappa r, \theta) = (W_0(\kappa r, \theta), \ldots, W_N(\kappa r, \theta))$, and $\mathcal{T}_N$ is the vector of functions $\mathcal{T}_N(\phi) = (\mathcal{I} - \mathcal{X}_\Gamma(\phi))\,(1, \mathrm{e}^{\mathrm{i}\phi}, \ldots, \mathrm{e}^{\mathrm{i}N\phi})$.

Further computational efficiency can be achieved by representing the fundamental solution as an expansion of Bessel functions. Combining Eqs. (39) and (42) and writing the Neumann function in Eq. (42) in terms of Bessel functions [1, Eq. (9.1.89)] yields:

$$\begin{aligned} h_g(x, 0) &= \sum_{n=0}^{\infty} 2\pi\hat{g}_n(0, \kappa)\,\mathrm{e}^{\mathrm{i}n(\theta+(\pi/2))}\,J_n(\kappa r) \\ &= \left[\frac{\mathrm{i}}{4} - \frac{1}{2\pi}\left(\ln\frac{\kappa r}{2} + \gamma\right)\right] J_0(\kappa r) + \frac{1}{\pi}\sum_{m=1}^{\infty}\frac{(-1)^m}{m}J_{2m}(\kappa r). \end{aligned} \tag{44}$$

for $x = r(\cos\theta, \sin\theta) \in \delta\Omega_0$: The scalar γ is Euler's constant. At first glance, since both sides of Eq. (44) involve expansions in terms of integral order Bessel functions, it might seem fruitful to obtain explicit expressions for the coefficients $\hat{g}_n(0, \kappa)$ by simply matching terms. This leads to coefficients $\hat{g}_n(0, \kappa)$ that depend on the spatial variables r and θ. In order to approximate the fundamental solution *everywhere* on some closed curve $\partial\Omega_0$ it is still necessary to solve the optimization problem (Eq. (43)).

Sampling the fundamental solution along the boundary of the generating approximation domain shown in Fig. 1(a) is particularly simple since with this domain one can exploit the radial symmetry. Care must be taken, however, to ensure that the radial components of the curve $\partial\Omega_0$ are sampled at a high enough rate relative to the wavenumber κ. Since, for every wavenumber κ, the total field satisfies the Dirichlet boundary condition $u = 0$ on $\partial\Omega$, we expect the sum of the modulus squared of the total field over all sampled wavenumbers to also be small in a neighborhood of the boundary. The images we construct are thus given by:

$$f(z_i) = \sum_{k=1}^{K}\sum_{j=1}^{J}|u^{\mathrm{s}}_*(z_i, \hat{\eta}_j, \kappa_k) + u^{\mathrm{i}}(z_i, \hat{\eta}_j, \kappa_k)|^2. \tag{45}$$

at points $z_i \in \mathcal{G}$ $(i \in \mathbb{N})$, the computational grid, where us $u^{\mathrm{s}}_*(z_i, \hat{\eta}_j, \kappa_k)$ is an approximation to the scattered field for each sampled direction $\hat{\eta}_j$, $(j \in \mathbb{N})$ and each frequency κ_k, $(k \in \mathbb{N})$.

Reconstructions using the point source method are accomplished in the following series of steps.

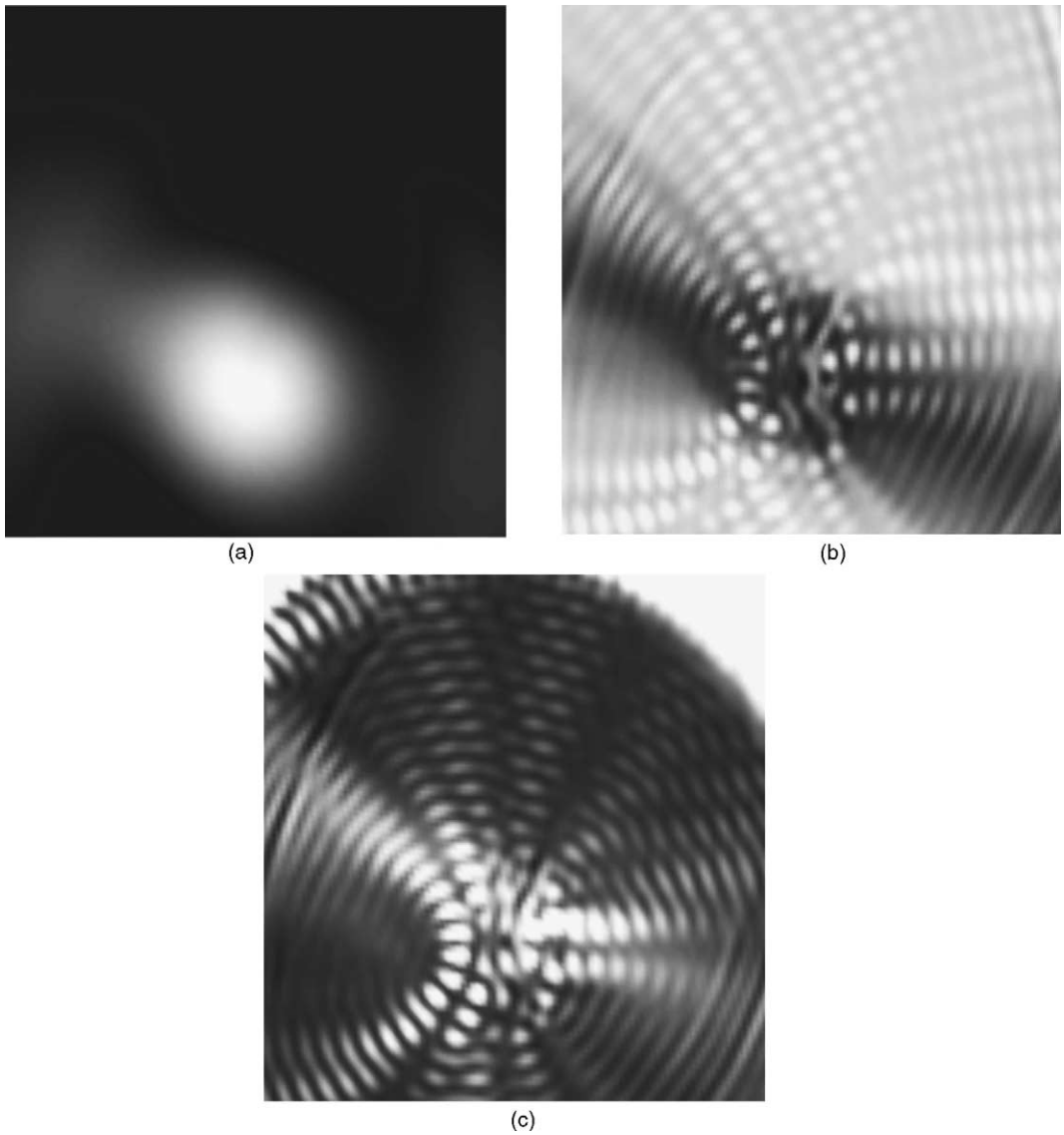

Fig. 3. Plots of the values $f(z_i)$ calculated via Eq. (45) for full aperture, $\Gamma = \mathbb{S}$, far-field data sampled at 128 points, 1 incident field with direction $7\pi/8$, and 16 wavenumbers evenly spaced on the interval [0.75, 10]. (a) Reconstruction using the physical optics density $\tilde{g}$ (see Eq. (30)) in Step 2 of Algorithm 1, rather than g_*. (b) Reconstruction with the point source method with density g_* calculated by using the first term of the Fourier series expansion of g_*. (c) Reconstruction with the point source method with density g_* calculated by using the exact optimization problem (Eq. (17)). For both (b) and (c), the regularization parameter $\alpha = 10^{-8}$. The corresponding approximation domain is shown in Fig. 1(a) with parameter values $R_1 = 0.07$, $R_2 = 6$, $\theta_\epsilon = 10^{-16}$.

Algorithm 1 (Multifrequency point source method).

Step 1 (Generating density $g * (\hat{y}, 0, \kappa)$). Set up the generating approximation domain Ω_0 and, at each frequency κ_k, solve the minimization problem Eq. (17) or (43) for the generating density $g_*(-\hat{y}_l, 0, \kappa_k)$ corresponding to the far-field measurements $u^\infty(\hat{y}_l, \hat{\eta}, \kappa_k)$ $(l, k \in \mathbb{N})$.

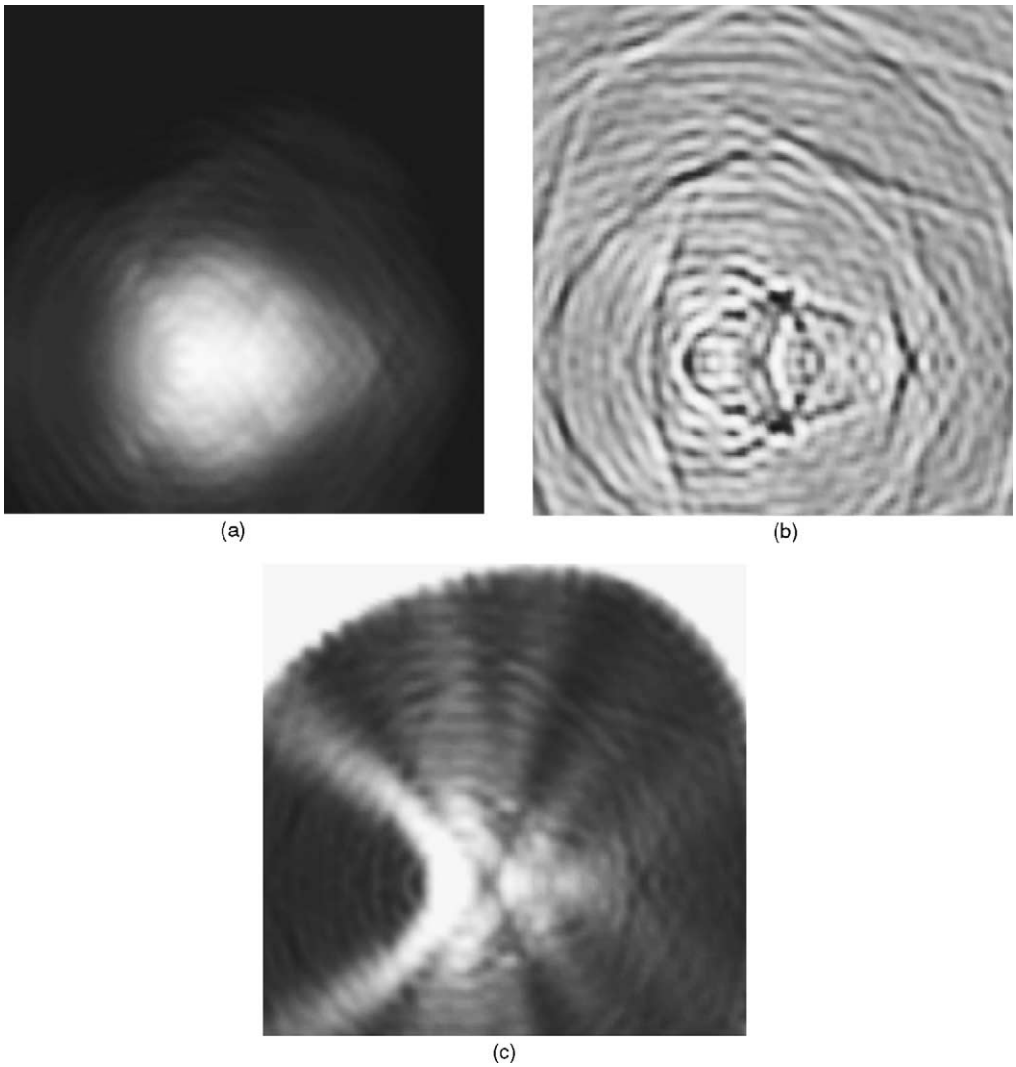

Fig. 4. Plots of the values $f(z_i)$ calculated via Eq. (45) for quarter aperture, $\Gamma = \pi/2$, incident fields evenly spaced on the interval $[0, 2\pi]$, and 8 wavenumbers evenly spaced on the interval [0.75, 10]. (a) Reconstruction using the physical optics density $\tilde{g}$ (see Eq. (30)) in Step 2 of Algorithm 1, rather than g_*. (b) Reconstruction with the point source method with density g_* calculated by using the first term of the Fourier series expansion of g_*. (c) Reconstruction with the point source method with density g_* calculated by using the exact optimization problem (Eq. (17)). For both (b) and (c), the regularization parameter $\alpha = 10^{-8}$ and the penalty parameter $\tilde{\alpha} = 20$. The corresponding approximation domain is shown in Fig. 1(a) with parameter values $R_1 = 0.07$, $R_2 = 6$, $\theta_\epsilon = 10^{-16}$.

Step 2 (Backprojection). At points $z_i \in \mathcal{G}$ $(i \in \mathbb{N})$; the computational grid, calculate the approximation to the scattered field $u_*^s(z_i, \hat{\eta}_j, \kappa_k)$ for each direction $\hat{\eta}_j$, $(j \in \mathbb{N})$ and each frequency κ_k, $(k \in \mathbb{N})$.

Step 3 (Integration). Add the modulus squared of all approximated total fields, that is, for each z_i compute $f(z_i)$ defined by Eq. (45).

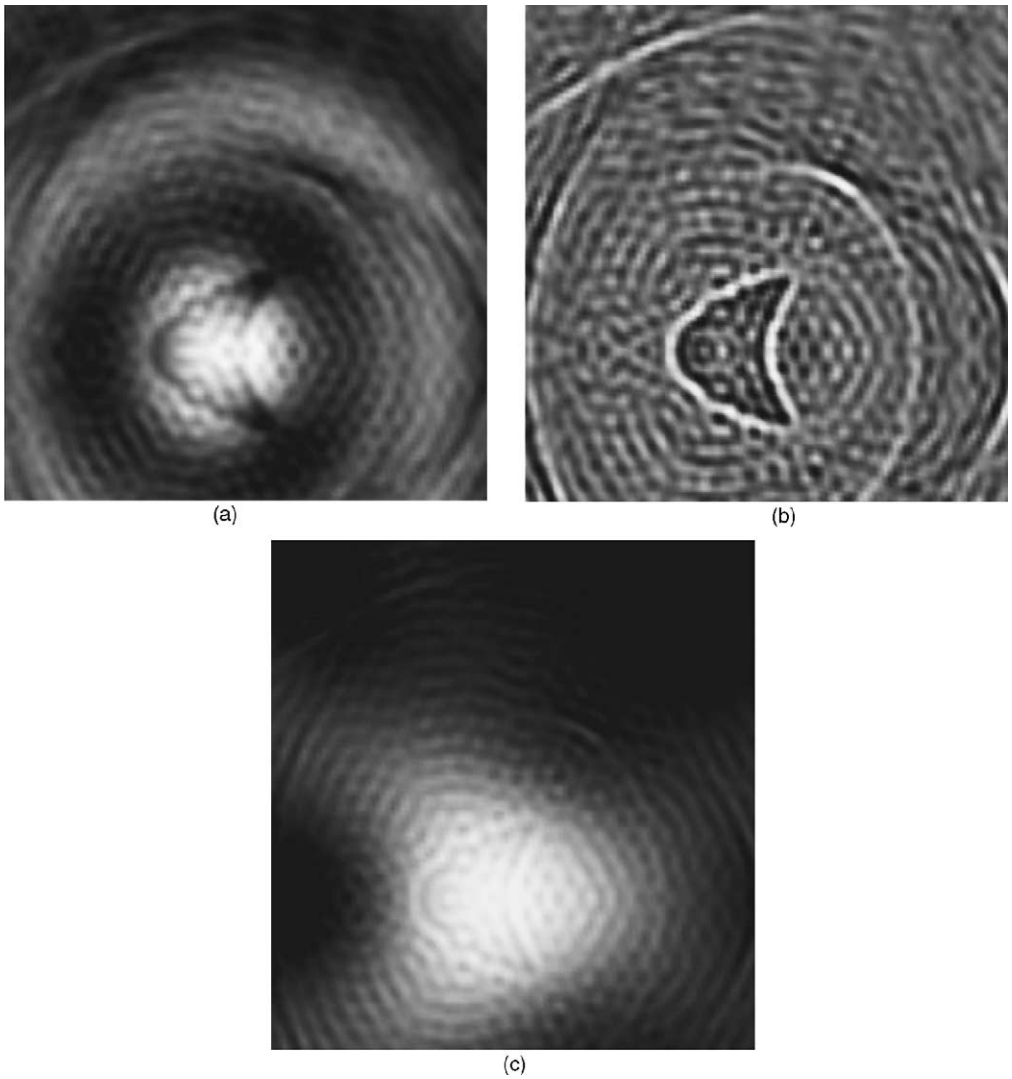

Fig. 5. Plots of the values $f(z_i)$ calculated via Eq. (45) for limited aperture, $\Gamma = (0, \pi/16)$, 32 incident fields evenly spaced on the interval $[0, 2\pi]$, and 16 wavenumbers evenly spaced on the interval [0.75, 10]. (a) Reconstruction using the physical optics density $\tilde{g}$ (see Eq. (30)) in Step 2 of Algorithm 1, rather than g_*. (b) Reconstruction with the point source method with density g_* calculated by using the first term of the Fourier series expansion of g_*. (c) Reconstruction with the point source method with density g_* calculated by using the exact optimization problem (Eq. (17)). For both (b) and (c), the regularization parameter $\alpha = 10^{-8}$ and the penalty parameter $\tilde{\alpha} = 20$. The corresponding approximation domain is shown in Fig. 1(a) with parameter values $R_1 = 0.07$, $R_2 = 6$, $\theta_\epsilon = 10^{-16}$.

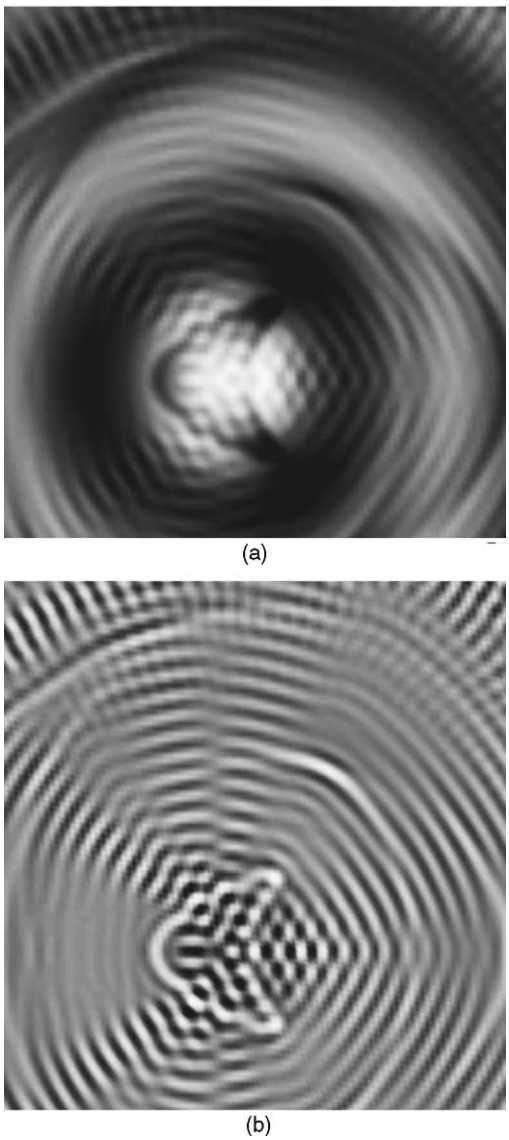

Fig. 6. Backscattering with 128 incident fields evenly spaced on the interval $[0, 2\pi]$, and 16 wavenumbers evenly spaced on the interval [0.75, 10]. (a) Reconstruction using the physical optics density $\tilde{g}$ given by Eq. (33) in Step 2 of Algorithm 1, rather than g_* given by Eq. (37). (b) Reconstruction with the point source method for density g_* given by Eqs. (36) and (37).

For our simulations, we use a kite-shaped sound-soft obstacle used in Section 3.5 in [5]. This is shown in Fig. 1(b). The parameter values for the approximation domain shown in Fig. 1(a) are the following: $R_1 = 0.07$, $R_2 = 6$, $\theta_\epsilon = 10^{-16}$.

Reconstructions with the point source method are shown with densities g_* calculated via the exact optimization problem Eq. (17) and also using the first term of the Fourier series expansion of g_*, that is solving Eq. (43) with $N = 0$. In each, the regularization parameter $\alpha = 10^{-8}$ and the penalty parameter

$\tilde{\alpha} = 20$. These reconstructions are compared to reconstructions using the physical optics density $\tilde{g}$ (see Eq. (30)) in Step 2 of Algorithm 1, rather than g_*. The figures show reconstructions for four different regimes: (Fig. 3) full aperture, $\Gamma = \mathbb{S}$, sampled at 128 points, 1 incident field, and 16 wavenumbers evenly spaced on the interval [0.75, 10]; (Fig. 4) quarter aperture, $\Gamma = \pi/2$, sampled at 32 points, 8 incident fields evenly spaced on the interval $[0, 2\pi]$, and eight wavenumbers evenly spaced on the interval [0.75, 10]; (Fig. 5) limited aperture, $\Gamma = (0, \pi/16)$ sampled at 4 points, 32 incident fields evenly spaced on the interval $[0, 2\pi]$, and 16 wavenumbers evenly spaced on the interval [0.75, 10]; and (Fig. 6) backscattering with 128 incident fields evenly spaced on the interval $[0, 2\pi]$, and 16 frequencies evenly spaced on the interval [0.75, 10]. In each of the experiments above, the same number of data points is used, that is, the number of far-field measurements times the number of incident fields times the number of frequencies used is always equal to 2048.

Our numerical results illustrate that the critical factor for reconstructions in multifrequency settings is the frequency dependence of the filter. Our results also show that the frequency dependence encoded in filters calculated by solving Eq. (17) or (43) delivers higher quality reconstructions than those generated with filters suggested by classical, high-frequency techniques. The Fourier series expansions explored here, together with a particular generating approximation domain (Fig. 1(a)) allow efficient implementations of the point source method with multifrequency data.

References

[1] M. Abramowitz, I.A. Stegun, Handbook of Mathematical Functions, 9th ed., Dover, New York, 1972.
[2] H.D. Albert, A.G. Ramm, Scattering amplitude and algorithm for solving the inverse scattering problem for a class of non-convex obstacles, J. Math. Anal. Appl. 117 (1986) 570–597.
[3] N.N. Bojarski, A Survey of the physical optics inverse scattering identity, IEEE Trans. Ant. Prop. AP-20 (1982) 980–989.
[4] D. Colton, A. Kirsch, A simple method for solving inverse scattering problems in the resonance region, Inverse Problems 12 (4) (1996) 383–393.
[5] D. Colton, R. Kress, Inverse Acoustic and Electromagnetic Scattering Theory, 2nd ed., Springer-Verlag, Berlin, 1998.
[6] D. Colton, P. Monk, A novel method for solving the inverse scattering problem for time-harmonic waves in the resonance region, SIAM J. Appl. Math. 45 (1985) 1039–1053.
[7] D. Colton, P. Monk, A novel method for solving the inverse scattering problem for time-harmonic waves in the resonance region II, SIAM J. Appl. Math. 46 (1986) 506–523.
[8] D. Colton, B.D. Sleeman, Uniqueness theorems for the inverse problem of acoustic scattering, IMA J. Appl. Math. 31 (1983) 253–259.
[9] I.S. Gradshteyn, I.M. Ryzhik, Table of Integrals, Series, and Products, 4th ed., Academic Press, London, 1965.
[10] A. Kirsch, R. Kress, A numerical method for an inverse scattering problem, in: H.W. Engl, C.W. Groetsch (Eds.), Inverse Problems, Academic Press, Orlando, 1987, pp. 279–290.
[11] R. Kress, Integral equation methods in inverse acoustic and electromagnetic scattering, in: D.B. Ingham, L.C. Wrobel (Eds.), Boundary Integral Formulations for Inverse Analysis, Computational Mechanics Publications, South Hampton, UK, 1997, pp. 67–92.
[12] R. Leis, Initial-boundary value and scattering problems in mathematical physics, in: Partial Differential Equations and Calculus of Variations, Lecture Notes in Mathematics, vol. 1357, Springer, Berlin, 1988, pp. 23–60.
[13] R. Lies, Initial Boundary Value Problems in Mathematical Physics, Teubner, Stuttgart, 1986.
[14] D.R. Luke, J.V. Burke, R.G. Lyon, Optical wavefront reconstruction: theory and numerical methods, SIAM Rev. 44 (2002) 169–224.
[15] D.R. Luke, R. Potthast, Image processing for limited aperture inverse acoustic obstacle scattering, Pacific Institute for the Mathematical Sciences Preprint (PIMS-03-12), Download: http://www.pims.math.ca/publications/preprints/.
[16] D.R. Luke, R. Potthast, The no response test—a sampling method for inverse scattering problems, SIAM J. Appl. Math. 63 (4) (2003) 1292–1312.

[17] F. Natterer, The Mathematics of Computerized Tomography, Wiley, New York, 1986.
[18] R. Potthast, A fast new method to solve inverse scattering problems, Inverse Problems 12 (1996) 731–742.
[19] R. Potthast, A point-source method for inverse acoustic and electromagnetic obstacle scattering problems, IMA J. Appl. Math. 61 (1998) 119–140.
[20] R. Potthast, Point Sources and Multipoles in Inverse Scattering Theory, Chapman & Hall, London, 2001.
[21] A.E. Yagel, Differential and integral methods for multidimensional inverse scattering problems, J. Math. Phys. 27 (1986) 2584–2591.